# Exploring Zeptosecond Quantum Equilibration Dynamics: From Deep-Inelastic to Fusion-Fission Outcomes in $^{58}$Ni + $^{60}$Ni Reactions

E. Williams,[1,*] K. Sekizawa,[2] D. J. Hinde,[1] C. Simenel,[1] M. Dasgupta,[1] I. P. Carter,[1] K. J. Cook,[1] D. Y. Jeung,[1] S. D. McNeil,[1] C. S. Palshetkar,[1,†] D. C. Rafferty,[1] K. Ramachandran,[1,‡] and A. Wakhle[1]

[1]*Department of Nuclear Physics, Research School of Physical Sciences and Engineering, The Australian National University, Canberra, ACT 2601, Australia*

[2]*Faculty of Physics, Warsaw University of Technology, ulica Koszykowa 75, 00-662 Warsaw, Poland*

(Received 16 August 2017; revised manuscript received 27 October 2017; published 10 January 2018)

Energy dissipative processes play a key role in how quantum many-body systems dynamically evolve toward equilibrium. In closed quantum systems, such processes are attributed to the transfer of energy from collective motion to single-particle degrees of freedom; however, the quantum many-body dynamics of this evolutionary process is poorly understood. To explore energy dissipative phenomena and equilibration dynamics in one such system, an experimental investigation of deep-inelastic and fusion-fission outcomes in the $^{58}$Ni + $^{60}$Ni reaction has been carried out. Experimental outcomes have been compared to theoretical predictions using time dependent Hartree-Fock and time dependent random phase approximation approaches, which, respectively, incorporate one-body energy dissipation and fluctuations. Excellent quantitative agreement has been found between experiment and calculations, indicating that microscopic models incorporating one-body dissipation and fluctuations provide a potential tool for exploring dissipation in low-energy heavy ion collisions.

DOI: 10.1103/PhysRevLett.120.022501

The dynamic evolution of perturbed quantum many-body systems toward equilibrium is a topic of great interest in many fields, including quantum information [1], condensed matter [2–5], and nuclear physics [6–10]. Energy dissipation—the transfer of energy from collective motion to internal or external degrees of freedom (d.o.f.)—shapes this dynamic evolution, playing a significant role in whether and how such complex systems achieve full equilibration. To date, a great deal of effort has focused on quantum systems in which energy dissipation is brought about via contact with an external environment (e.g., gas, photons, etc.) [11,12]. Much less is known about energy dissipation that arises from internal d.o.f. [2,5,13].

One testing ground for the exploration of energy dissipation due to internal d.o.f. can be found in heavy ion collisions. The nuclear collision process results in a closed composite quantum system that is isolated from external environments during the time of the collision (a time scale of several zeptoseconds, prior to particle emission), rapidly evolves toward equilibration in many d.o.f., and undergoes significant excitation and internal rearrangement throughout the equilibration process. Through the manipulation of collision entrance channel parameters (projectile-target combinations and energies), a range of factors with the potential to affect energy dissipation can be explored. Typical time scales for energy dissipation in such systems could, in principle, vary from isospin and mass equilibration times on the order of 0.3–0.5 [14,15] and ~5 zs [16,17], respectively.

In nuclear reactions, the observation of the total kinetic energy of the reaction products (TKE) offers a direct measure of energy dissipation. The observation of the masses of reaction products via direct or indirect methods offers a measure of system equilibration in a key d.o.f. and can be used to explore fluctuations in reaction product masses as a function of TKE. One or both observables have often been used to explore energy dissipative outcomes in nuclear physics (see, e.g., [18]). In this work, we will explore the TKE and mass d.o.f. for binary outcomes of collisions between $^{58}$Ni and $^{60}$Ni at energies near the Coulomb barrier.

We have chosen to study low-energy collisions between $^{58}$Ni and $^{60}$Ni for several reasons. First, the entrance channel is close to symmetry. This means we can focus on quantum fluctuations without taking into account macroscopic mass drift effects, while avoiding the experimental difficulties that come with symmetric reactions (e.g., normalization with Mott scattering, indistinguishability of projectilelike and targetlike outcomes). Second, the system is relatively heavy—meaning it truly qualifies as a composite many-body system—but is still light enough that the charge product, and thus, the Coulomb repulsion, of the system is fairly small, allowing for long contact times. Most importantly, the system is accessible via both experiment and theory, using stable heavy ion beams in the former case and microscopic approaches employing one-body dissipation [time-dependent Hartree Fock (TDHF) [19]]

 

and fluctuations [time-dependent random phase approximation (TDRPA) [20]] in the latter.

The $^{58}$Ni + $^{60}$Ni experiment was performed at the ANU Heavy Ion Accelerator Facility using the 14UD tandem accelerator, CUBE two-body fission spectrometer [21] and two monitor detectors at 18° for cross section normalization. The $^{58}$Ni beam impinged upon the 60 $\mu$g/cm$^2$-thick $^{60}$Ni target for 20 separate beam energies ranging from ~194 to 270 MeV. The CUBE spectrometer's two large-area multiwire proportional counters (each 27.9 cm wide, 35.7 cm high) were placed at forward angles 45° relative to the beam axis and a distance of 22.24 cm from the target. The detectors provided energy loss, time of flight, and $(x, y)$ position information with a resolution of 1 mm. From this, a full kinematic reconstruction of each two-body event was performed using the kinematic coincidence method [21,22], providing TKE, mass ratio $M_R = M_1/(M_1 + M_2)$, where $M_i$ are the masses of the two fission fragments, and scattering angle information.

Calibrations were performed with a $^{58}$Ni beam of 158.4 MeV bombarding $(50, 60)$-$\mu$g/cm$^2$ $^{58,60}$Ni targets. Mott or Rutherford scattering were used to calibrate the geometry of the setup, define the mass ratio resolution of CUBE, and provide a solid angle calibration for cross section measurements.

Figure 1 shows the evolution of mass ratio distributions observed for $^{58}$Ni + $^{60}$Ni with $E/V_B$, or energy $E$ relative to the experimental fusion barrier $V_B = 96.87$ MeV [23] in the center-of-mass frame. In Fig. 1(a), an angular acceptance of $65° < \theta_{\mathrm{c.m.}} < 115°$ has been used to exclude regions where detector coverage is incomplete. The lowest

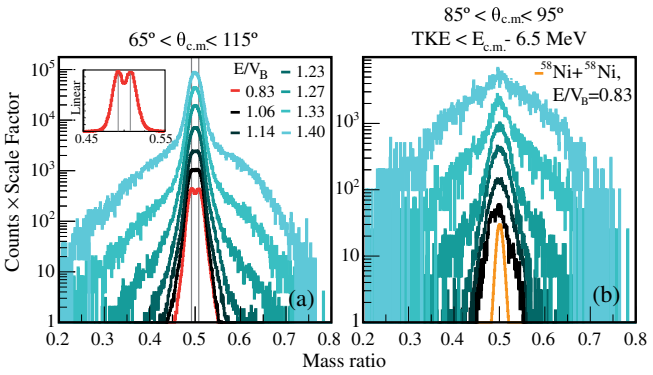


FIG. 1. Mass ratio distributions from the $^{58}$Ni + $^{60}$Ni reaction for a range of $E/V_B$. In (a), a $65° < \theta_{\mathrm{c.m.}} < 115°$ gate has been used to ensure full detector coverage. The thin vertical lines indicate the expected mass ratios for the projectile and target nuclei. The inset shows an enlarged version of the $E/V_B = 0.83$ mass ratio distribution on a linear scale. In (b), a gate has been placed on TKE that excludes 99% of the Rutherford scattered events, together with an $85° < \theta_{\mathrm{c.m.}} < 95°$ gate that isolates mass ratios corresponding to the region where fusion-fission events are expected to be found. The orange line shows $^{58}$Ni + $^{58}$Ni data at $E/V_B = 0.83$ without angle or TKE gate. No background subtraction has been applied to any of these mass distributions.

energy distribution (red line, $E/V_B = 0.83$) exhibits a double-peaked structure as highlighted by the linear scale inset of the same data. This is consistent with expectation for elastically scattered projectile ($M_R = 0.49$) and target ($M_R = 0.51$) nuclei. As $E/V_B$ is increased, the double peak becomes a single peak due to mass equilibration, and the previously narrow mass ratio distribution develops a second, wide component.

In Fig. 1(b), the wide component of the mass ratio distribution at higher energies is highlighted by applying two gates: one around $\theta_{\mathrm{c.m.}} = 90°$ that minimizes elastic and deep-inelastic events and one below TKE $= E_{\mathrm{c.m.}} -$ 6.5 MeV that excludes ~99% of the Rutherford scattering events. As beam energy increases, the narrow (wide) component of the mass ratio distribution decreases (increases) in yield. At the highest energy, almost no trace of the narrow component remains. For reference, the $^{58}$Ni + $^{58}$Ni mass ratio (orange) shows the experimental mass ratio resolution for an individual nuclide.

To identify the various reaction outcomes contributing to the mass ratio spectra in Fig. 1, the experimental TKE information must also be considered as it provides information on whether energy dissipation has occurred. In Fig. 2, $\theta_{\mathrm{c.m.}}$ versus TKE is shown for three representative energies (overlaid with calculations; to be discussed below). The highest intensity (light yellow) regions at high TKE values are consistent with elastic scattering energies. Events with lower TKE values, present in each case [for example, below ≈110 MeV in Fig. 1(a)], provide evidence of energy dissipative reaction processes as early as $E/V_B = 1.14$. Such events could correspond to either deep-inelastic or fusion-fission outcomes.

The main distinguishing experimental features for deep-inelastic and fusion-fission processes here are that fusion-fission outcomes should have full energy dissipation [e.g., appear in a flat TKE band, like that seen in Fig. 2(c) around ≈80 MeV] and exhibit a wide mass distribution (indicating that significant mass transfer has occurred), while deep-inelastic collisions only need to show energy dissipation relative to expected elastic scattering TKE values and may involve only a small amount of mass transfer (i.e., the incoming and outgoing reaction channel masses can be similar). From Fig. 1(b), it is clear that the wide mass ratio component of the data (which is consistent with fusion-fission) does not become important until $E/V_B \sim 1.27$. Based on the experimental information alone, it is unclear whether the wide mass ratio distributions observed in Fig. 1 are solely due to fusion-fission, a deep-inelastic process, or some combination of the two.

To explore the relationship between experimental observables ($\theta_{\mathrm{c.m.}}$, TKE) and impact parameter $b$, and to examine the origin of the wide mass ratio component, microscopic approaches TDHF and TDRPA have been used. TDHF is a mean-field approach incorporating one-body dissipation that has previously been used to explore

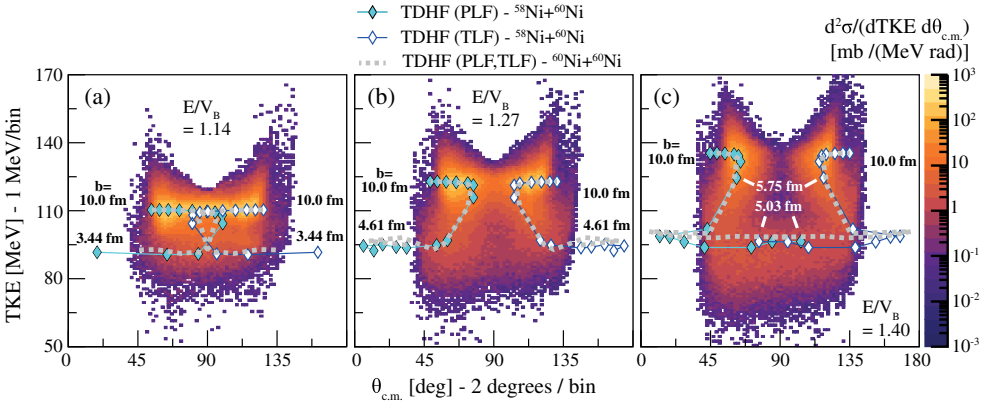


FIG. 2. Scattering angle $\theta_{\mathrm{c.m.}}$ vs TKE differential cross section distributions $d^2\sigma/(d\theta_{\mathrm{c.m.}}d\mathrm{TKE})$ for $^{58}\mathrm{Ni} + {}^{60}\mathrm{Ni}$ at (a) $E/V_B = 1.14$, (b) $E/V_B = 1.27$, and (c) $E/V_B = 1.40$ overlaid with ($\theta_{\mathrm{c.m.}}$, TKE) impact parameter trajectories calculated with TDHF. (Diamond symbols) $^{58}\mathrm{Ni} + {}^{60}\mathrm{Ni}$, where black diamonds are projectilelike fragments (PLF), white diamonds are targetlike fragments (TLF); (Dotted lines) $^{60}\mathrm{Ni} + {}^{60}\mathrm{Ni}$. Differential cross sections are only a lower limit outside of the range of $65° < \theta_{\mathrm{c.m.}} < 115°$ due to detector angular coverage. The impact parameter $b$ for selected points along the TDHF trajectories are shown.

dynamical reaction processes such as quasifission [10,24–30]. In this work, a 3D TDHF code [31,32], employing the SLy4d parametrization [33] of the Skyrme energy-density functional [34], has been used to explore reaction outcomes for $^{58,60}\mathrm{Ni} + {}^{60}\mathrm{Ni}$ at the three representative energies shown in Fig. 2. The code has been extended and also used for the TDRPA calculations.

TDHF calculations were performed for a reaction time scale of 13 zs, and the minimum impact parameter for each calculation set was chosen to correspond to the minimum value at which the dinuclear system was observed to reseparate into two components over this time scale. Below these minimum impact parameters, it is assumed that fusion is the most probable outcome—an assumption that is supported by calculated moments of inertia for impact parameters below the minimum range, which indicated convergence toward a compact system (see Supplemental Material [35]). The maximum impact parameter for all calculations was chosen to be 10 fm. In Fig. 2, each experimental data set has been overlaid with the results of these TDHF calculations. Each diamond pair represents the calculated average $\theta_{\mathrm{c.m.}}$ and TKE value obtained from a given impact parameter calculation for the $^{58,60}\mathrm{Ni} + {}^{60}\mathrm{Ni}$ reactions. Impact parameters corresponding to selected points along these trajectories in ($\theta_{\mathrm{c.m.}}$, TKE) space have been noted; we will henceforth call these trajectories in ($\theta_{\mathrm{c.m.}}$, TKE) space "impact parameter trajectories." Both reactions yield a similar evolution in ($\theta_{\mathrm{c.m.}}$, TKE) space. For the three representative calculations, the largest impact parameters (at high TKE values) result in little energy dissipation (yielding points near elastic scattering outcomes), while the smallest impact parameters (at low TKE values) exhibit significant energy dissipation. The impact parameters for each calculation are not evenly spaced to capture the rapid change in dynamics in the small impact parameter range.

As one can see from Figs. 2(a)–2(c), the TDHF impact parameter trajectories follow the trends in the data quite well over the full experimental angular range. Outcomes for small impact parameters exhibit increased energy dissipation and dinuclear system rotation before reseparation relative to outcomes for large impact parameters. In the calculations, we define contact time as the time during which the density overlap between the fragments is $\rho > 0.001$ fm$^{-3}$ (selected to provide a smooth evolution in contact time as a function of $b$, as discussed in [35]). This generally increases as $b$ decreases, thus allowing more time for both rotation and energy dissipation to occur.

So far, we have found that the reaction outcomes are characterized by (i) strong TKE-angle correlations and (ii) a transition between narrow and wide components in the fragment mass distributions. The next step is to investigate the correlation between energy dissipation and mass fluctuations in the fragments. Experimentally, we can achieve this by examining the evolution of $\sigma_{\mathrm{MR}}$, the standard deviation of a Gaussian fit to the mass ratio distribution along the TDHF impact parameter trajectories. To compare this to theory, we need to first examine the ability of microscopic theories to reproduce this evolution of $\sigma_{\mathrm{MR}}$ along the impact parameter trajectories shown in Fig. 2.

Because of its mean-field nature, TDHF is optimized to calculate the average of one-body observables (e.g., fragment mass, charge), but underestimates their fluctuations [36]. A realistic estimate of the latter can be obtained with TDRPA [20], an extension of TDHF that successfully reproduced mass distribution widths in $^{40}\mathrm{Ca} + {}^{40}\mathrm{Ca}$ [7]. The TDRPA dispersion formula can be derived from the stochastic mean-field approach [37]. TDRPA is used to calculate fluctuations in particle number $A$ in the fragments, which can be interpreted as a standard deviation $\sigma_A = (\bar{A^2} - \bar{A}^2)^{1/2}$ only in the case of symmetric collisions. $\sigma_A$ can then be used to compute the calculated equivalent of

$\sigma_{MR}$ by dividing by the compound nucleus mass number. As Fig. 2 showed, the TDHF trajectories for $^{58,60}Ni + {}^{60}Ni$ were found to be very similar; therefore, the calculated $^{60}Ni + {}^{60}Ni$ trajectories and $\sigma_{MR}$ values will be used in the discussion below. For completeness, we have also computed fragment mass fluctuations in $^{58}Ni + {}^{60}Ni$ with TDRPA, to see if the asymmetry is small enough to allow an interpretation of the TDRPA mass fluctuations as $\sigma_A$ in this system. The details of this calculation can be found in [35].

To compare calculations to observation, a series of scattering angle and TKE gates were placed on the data along the TDHF trajectories identified in Fig. 2. Each gate was centered on the $\theta_{c.m.}$ and TKE value resulting from each TDHF impact parameter calculation where detector coverage was complete. The gate widths were chosen as follows: (i) TKE gate widths were ≈5 MeV, corresponding to the observed full width at half maximum of the TKE for elastic scattering events in the $^{58}Ni + {}^{60}Ni$ calibration run at $E/V_B = 0.83$; and (ii) $\theta_{c.m.}$ gate widths were 5°, as this width yielded reasonable statistics in the mass distributions. The resulting experimental $\sigma_{MR}$ values are shown as a function of TDHF impact parameter $b$ in Fig. 3(a) for the highest energy measurement. Here, $\sigma_{MR}$ decreases sharply over a narrow impact parameter range. The largest $\sigma_{MR}$ values, found at the smallest impact parameters, correspond to mass ratio widths consistent with those observed for

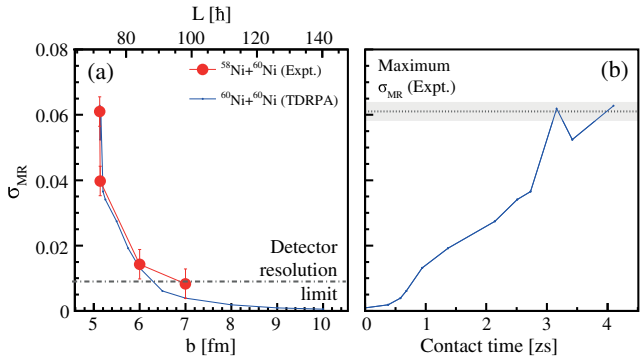


FIG. 3. (a) TDRPA and observed $\sigma_{MR}$ values are plotted as a function of calculated impact parameter $b$ for $E/V_B = 1.40$. For the experimental data, $\sigma_{MR}$ is obtained from a Gaussian fit of the mass ratio within a ($\theta_{c.m.}$,TKE) gate corresponding to the equivalent trajectory given by the symmetric calculation; the impact parameter for each point is assigned based on the symmetric trajectory. The error bars on the experimental points and the gray dashed line show the detector mass resolution obtained from the $\sigma_{MR}$ of the below-barrier $^{58}Ni + {}^{58}Ni$ data, corresponding to the detector mass ratio resolution for a single atomic mass. Because data points have been selected along the projectilelike branch of the trajectory, points at high TKE values (large $b$) are expected to approach the resolution limit. (b) TDHF contact time versus $\sigma_{MR}$ from TDRPA. The dotted line indicates maximum $\sigma_{MR}$ from experiment with the shaded region representing the detector mass ratio resolution.

fusion-fission outcomes in heavier systems (see, e.g., [22,38,39]).

The TDRPA results for $^{60}Ni + {}^{60}Ni$ are also shown in Fig. 3(a). The agreement between the theoretical (mass symmetric) and experimental $\sigma_{MR}$ is remarkable, considering the fact that the only input of TDRPA (and TDHF) is the choice of the effective interaction. This conclusion holds for all three energies. For the reaction at $E/V_B = 1.14$ and minimum impact parameter $b = 3.8$ fm, $\sigma_{MR,expt} = 0.027(9)$, and $\sigma_{MR,calc} = 0.017$; for the reaction at $E/V_B = 1.27$ and minimum impact parameter $b = 5.0$ fm, $\sigma_{MR,expt} = 0.025(9)$ and $\sigma_{MR,calc} = 0.017$. Experimental errors on $\sigma_{MR}$ given here originate from the detector resolution, as determined from the $^{58}Ni + {}^{58}Ni$ calibration data. In both cases, experimental $\sigma_{MR}$ values then decrease quickly to the CUBE resolution limit as $b$ is increased.

The TDHF and TDRPA calculations also reveal something about the wide mass component of the highest energy reaction that the experimental data cannot: the reaction time scale. As shown in Fig. 3(b), the widest calculated $\sigma_{MR}$ values result from reactions with longer contact times ($\gtrsim$3 zs). These calculated mass distribution widths are consistent with those observed for the wide mass component of our experimental data, supporting the idea that this wide mass component results from systems that have more time to undergo mass exchange prior to reseparation. This suggests that the wide mass ratio component of the experimental data could originate from both deep-inelastic and fusion-fission processes, where the ∼4 zs time scale applies to the former process and a much longer ($>10^{-20}$ s) time scale to the latter. Remarkably, the fact that the largest calculated mass ratio widths could be consistent with those expected for fusion-fission, where full mass equilibration has by definition occurred, also suggests that full mass equilibration can be achieved over a time scale of only ∼4 zs for this reaction. This time scale range is consistent with the 5–10 zs time scales observed for quasifission outcomes in some heavier systems [16,17,40].

In summary, this Letter illustrates the strong quantitative agreement between experiment and a quantum many-body approach including only a one-body dissipation mechanism for low-energy heavy ion collisions, supporting the idea that such approaches are highly appropriate for exploring energy dissipative processes in composite quantum many-body systems. The 4 zs time scale for the mass equilibrated deep-inelastic outcome, as calculated by TDRPA, suggests that the microscopic mechanisms driving mass equilibration can operate very rapidly in low-energy heavy ion reactions.

The authors thank the technical staff of the ANU Heavy Ion Accelerator Facility for their essential support during the experiments. The authors also acknowledge support from the Australian Research Council through Grants No. DE140100784, No. FT120100760,

No. FL110100098, No. DP130101569, No. DP140101337, and No. DP160101254; from the NCRIS program for accelerator operations; and from the Polish National Science Centre (NCN) Grant, Decision No. DEC-2013/08/A/ST3/00708. This work used computational resources of the HPCI system (HITACHI SR16000/M1) provided by Information Initiative Center (IIC), Hokkaido University, through the HPCI System Research Projects (Project IDs: hp140010, hp150081, hp160062, and hp170007).

*elizabeth.williams@anu.edu.au
†Present address: Department of Nuclear and Atomic Physics, Tata Institute of Fundamental Research, Mumbai 400 005 India.
‡Present address: Nuclear Physics Division, Bhabha Atomic Research Centre, Mumbai 400 085, India.

[1] D. Suter and G. A. Álvarez, Rev. Mod. Phys. **88**, 041001 (2016).
[2] A. Polkovnikov, K. Sengupta, A. Silva, and M. Vengalattore, Rev. Mod. Phys. **83**, 863 (2011).
[3] M. Gring, M. Kuhnert, T. Langen, T. Kitagawa, R. Rawer, M. Schreitl, I. Mazets, D. A. Smith, E. Demler, and J. Schmiedmayer, Science **337**, 1318 (2012).
[4] H. Aoki, N. Tsuji, M. Eckstein, M. Kollar, T. Oka, and P. Werner, Rev. Mod. Phys. **86**, 779 (2014).
[5] J. Eisert, M. Friesdorf, and C. Gogolin, Nat. Phys. **11**, 124 (2015).
[6] D. J. Hinde, M. Dasgupta, A. Diaz-Torres, and M. Evers, Nucl. Phys. **A834**, 117c (2010).
[7] C. Simenel, Phys. Rev. Lett. **106**, 112502 (2011).
[8] Y. Aritomo, K. Hagino, K. Nishio, and S. Chiba, Phys. Rev. C **85**, 044614 (2012).
[9] D. Lacroix and S. Ayik, Eur. Phys. J. A **50**, 95 (2014).
[10] A. S. Umar, V. E. Oberacker, and C. Simenel, Phys. Rev. C **92**, 024621 (2015).
[11] G. Barontini, R. Labouvie, F. Stubenrauch, A. Vogler, V. Guarrera, and H. Ott, Phys. Rev. Lett. **110**, 035302 (2013).
[12] I. de Vega and D. Alonso, Rev. Mod. Phys. **89**, 015001 (2017).
[13] G. Clos, D. Porras, U. Warring, and T. Schaetz, Phys. Rev. Lett. **117**, 170401 (2016).
[14] A. Jedele, A. B. McIntosh, K. Hagel, M. Huang, L. Heilborn, Z. Kohley, L. W. May, E. McCleskey, M. Youngs, A. Zarrella *et al.*, Phys. Rev. Lett. **118**, 062501 (2017).
[15] A. S. Umar, C. Simenel, and W. Ye, Phys. Rev. C **96**, 024625 (2017).
[16] J. Tōke, B. Bock, G. X. Dai, A. Gobbi, S. Gralla, K. D. Hildenbrand, J. Kuzminski, W. Müller, A. Olmi, and H. Stelzer, Nucl. Phys. **A440**, 327 (1985).
[17] R. du Rietz, E. Williams, D. J. Hinde, M. Dasgupta, M. Evers, C. J. Lin, D. H. Luong, C. Simenel, and A. Wakhle, Phys. Rev. C **88**, 054618 (2013).
[18] W. U. Schröder and J. R. Huizenga, in *Treatise on Heavy-Ion Science*, edited by D. Bromley (Plenum, New York, 1984), Vol. 2, p. 115.
[19] P. A. M. Dirac, Proc. Cambridge Philos. Soc. **26**, 376 (1930).
[20] R. Balian and M. Véneroni, Phys. Lett. **136B**, 301 (1984).
[21] D. J. Hinde, M. Dasgupta, J. R. Leigh, J. C. Mein, C. R. Morton, J. O. Newton, and H. Timmers, Phys. Rev. C **53**, 1290 (1996).
[22] R. Rafiei, R. G. Thomas, D. J. Hinde, M. Dasgupta, C. R. Morton, L. R. Gasques, M. L. Brown, and M. D. Rodriguez, Phys. Rev. C **77**, 024606 (2008).
[23] M. D. Rodríguez, M. L. Brown, M. Dasgupta, D. J. Hinde, D. C. Weisser, T. Kibédi, M. A. Lane, P. J. Cherry, A. G. Muirhead, R. B. Turkentine *et al.*, Nucl. Instrum. Methods Phys. Res., Sect. A **614**, 119 (2010).
[24] C. Simenel, D. J. Hinde, R. du Rietz, M. Dasgupta, M. Evers, C. J. Lin, D. H. Luong, and A. Wakhle, Phys. Lett. B **710**, 607 (2012).
[25] C. Simenel, Eur. Phys. J. A **48**, 152 (2012).
[26] A. Wakhle, C. Simenel, D. J. Hinde, M. Dasgupta, M. Evers, D. H. Luong, R. du Rietz, and E. Williams, Phys. Rev. Lett. **113**, 182502 (2014).
[27] V. E. Oberacker, A. S. Umar, and C. Simenel, Phys. Rev. C **90**, 054605 (2014).
[28] K. Hammerton, Z. Kohley, D. J. Hinde, M. Dasgupta, A. Wakhle, E. Williams, V. E. Oberacker, A. S. Umar, I. P. Carter, K. J. Cook *et al.*, Phys. Rev. C **91**, 041602 (2015).
[29] K. Sekizawa and K. Yabana, Phys. Rev. C **93**, 054616 (2016).
[30] A. S. Umar, V. E. Oberacker, and C. Simenel, Phys. Rev. C **94**, 024605 (2016).
[31] K. Sekizawa and K. Yabana, Phys. Rev. C **88**, 014614 (2013).
[32] K. Sekizawa and K. Yabana, Phys. Rev. C **93**, 029902(E) (2016).
[33] K.-H. Kim, T. Otsuka, and P. Bonche, J. Phys. G **23**, 1267 (1997).
[34] T. H. R. Skyrme, Philos. Mag. **1**, 1043 (1956).
[35] See Supplemental Material at http://link.aps.org/supplemental/10.1103/PhysRevLett.120.022501 for an extended discussion of the TDHF and TDRPA calculations presented in this work.
[36] C. H. Dasso, T. Dossing, and H. C. Pauli, Z. Phys. A **289**, 395 (1979).
[37] S. Ayik, Phys. Lett. B **658**, 174 (2008).
[38] G. N. Knyazheva, E. M. Kozulin, R. N. Sagaidak, A. Y. Chizhov, M. G. Itkis, N. A. Kondratiev, V. M. Voskressensky, A. M. Stefanini, B. R. Behera, L. Corradi *et al.*, Phys. Rev. C **75**, 064602 (2007).
[39] E. Williams, D. J. Hinde, M. Dasgupta, R. du Rietz, I. P. Carter, M. Evers, D. H. Luong, S. D. McNeil, D. C. Rafferty, K. Ramachandran *et al.*, Phys. Rev. C **88**, 034611 (2013).
[40] R. du Rietz, D. J. Hinde, M. Dasgupta, R. G. Thomas, L. R. Gasques, M. Evers, N. Lobanov, and A. Wakhle, Phys. Rev. Lett. **106**, 052701 (2011).